Available online at www.sciencedirect.com
SCIENCE DIRECT
Journal of Catalysis 230 (2005) 484–492
JOURNAL OF CATALYSIS
www.elsevier.com/locate/jcat

Oxidative dehydrogenation of ethylbenzene over vanadia-alumina catalysts in the presence of nitrous oxide: structure-activity relationship

N.R. Shiju, M. Anilkumar, S.P. Mirajkar, C.S. Gopinath, B.S. Rao, C.V. Satyanarayana *

Catalysis Division, National Chemical Laboratory, Dr. Homi Bhabha Road, Pune 411 008, India

Received 18 June 2004; revised 18 December 2004; accepted 7 January 2005

Abstract

A series of vanadia-alumina catalysts with different vanadia contents were prepared by a wet impregnation method. The influence of the local structure of vanadia in these catalysts on the oxidative dehydrogenation of ethylbenzene with nitrous oxide was investigated. The use of N_2O as a co-feed remarkably enhanced the styrene yield compared with the use of N_2. Characterization of these vanadia catalysts by XRD, FTIR, UV–vis, TPR, XPS, and ^{51}V NMR techniques suggests that the nature of the VO_x species depends on the vanadia loading; the predominant species are monomeric vanadia at lower loadings, two-dimensional polyvanadates at intermediate loadings, and bulk-like V_2O_5 and $AlVO_4$ at higher loadings. The rate of oxidative dehydrogenation (ODH) of ethylbenzene per vanadium atom increases with vanadia loading and reaches a maximum at 10 wt%, the loading at which the surface predominantly contains polyvanadate species. The observed variation in the selectivity of products with vanadium loading indicates that the monomeric V^{5+} species favors dehydrogenation, whereas bulk-like V_2O_5 preferentially participates in the dealkylation of ethylbenzene. The vanadium species remains at a higher oxidation state in the presence of N_2O, leading to a higher styrene yield, than in a N_2 atmosphere. The ODH turnover rates increased with decreasing energy of the absorption edge in the UV–vis spectrum, at low VO_x coverages of less than one monolayer on the Al_2O_3 surface.

Keywords: Oxidative dehydrogenation; Ethylbenzene; Nitrous oxide; Styrene; Alumina; Vanadia; Polyvanadates; Absorption edge energy

1. Introduction

Styrene, an important monomer for synthetic polymers, is produced commercially by means of the dehydrogenation of ethylbenzene (EB), with iron oxide as a catalyst. The reaction is endothermic and EB conversion is limited by thermodynamic equilibrium [1]. In commercial operation (873–903 K), an excess amount of superheated steam is used to provide the energy needed by the reaction, to dilute the reactant and to reduce catalyst coking [2]. Since the current process is equilibrium limited and energy intensive, there is a strong incentive for the development of an oxidative dehydrogenation process.

The advantage of an oxidative dehydrogenation process is that it can be operated at a lower temperature, as it is exothermic. In addition, the conversion would not be equilibrium limited. However, the use of oxygen in this process can lead to deep oxidation of EB to CO_x. Sulfur dioxide has been proposed as an alternative mild oxidizing agent [3]; however, its use is not attractive because of the formation of toxic and corrosive by-products like CS_2, COS, and benzothiophene. CO_2 has also been proposed as an alternative oxidizing agent [4–9]. The fast deactivation of the catalysts, as a result of the formation of carbonaceous deposits, is a major drawback in this case [10].

Lopez Nieto et al. [11] used N_2O as an oxidizing agent for the oxidative dehydrogenation of *n*-butane and found that selectivity for olefins was higher when compared with molecular oxygen as an oxidant. Recently, Kustrowski et al. [12] studied the coupling of N_2O decomposition with ethylbenzene dehydrogenation and obtained promising results with respect to the EB and N_2O conversions. N_2O is also utilized for the oxidative dehydrogenation of propane, result-

* Corresponding author. Fax: +91 20 25893761.
E-mail address: satya@cata.ncl.res.in (C.V. Satyanarayana).

0021-9517/$ – see front matter
doi:10.1016/j.jcat.2005.01.010

ing in an enhanced propene selectivity (for the same degree of propane conversion) compared with O_2 as the oxidizing agent [13]. Use of N_2O is of additional interest because this gas, which causes global warming, is effectively utilized in this reaction. N_2O, which is a by-product of the production of adipic and nitric acids, has an average lifetime of about 150 years and exerts a net greenhouse effect that is about 300 times that of CO_2 [14].

Previous studies have demonstrated that supported vanadia systems exhibit high activity and selectivity for alkane oxydehydrogenation [15–19]. The molecular structure and reactivity of alumina-supported vanadia catalysts have been extensively investigated in recent years for the selective oxidation of hydrocarbons [20–40]. The vanadia species on the alumina surface range from highly dispersed monovanadates to dimeric tetrahedral, polymeric vanadia, and V_2O_5 crystallites depending on the vanadia content. The rate of the reaction and selectivity depend significantly on the superficial structure of the vanadia species present on the surface [39–43].

In the present study, we report the catalytic properties of VO_x/γ-Al_2O_3 for the ODH of ethylbenzene, with N_2O as the oxidant. The catalysts were prepared by a wet impregnation method and characterized by X-ray diffraction, BET surface area, temperature-programmed reduction in hydrogen, XPS, FTIR, UV–vis, and ^{51}V NMR spectroscopy. We have tried to correlate the local structure of vanadia in these catalysts with their activity and selectivity.

2. Experimental

VO_x/Al_2O_3 catalysts were prepared by impregnation of γ-Al_2O_3 (113 $m^2\,g^{-1}$; Alfa Products, UK) with NH_4VO_3 dissolved in an aqueous solution of oxalic acid (1:2 weight ratio). After impregnation, the samples were dried in air at 383 K for 12 h and calcined in air at 823 K for 4 h. Different samples are designated in the text as $n\,VO_x/Al_2O_3$, where n is an integer corresponding to the nominal loading of vanadia on γ-Al_2O_3 as percentage by weight of V_2O_5. The BET surface areas of the samples, S_{BET}, were measured by nitrogen physisorption at 77 K with a surface area analyzer, Quantachrome NOVA 1200. The catalyst samples were evacuated at 573 K for 3 h before N_2 physisorption measurements. VO_x surface densities were calculated from BET surface areas and vanadium contents determined by ICP.

Powder X-ray diffraction (XRD) patterns were obtained on a Rigaku Miniflex diffractometer with Cu-K_α radiation ($\lambda = 0.15406$ nm, 30 kV, 15 mA). Fourier transform-infrared spectra of the samples were recorded (Shimadzu 8300 FTIR) at ambient conditions. The spectra were recorded with the use of thin circular discs we made by pressing a mixture of catalyst samples and KBr.

The temperature-programmed reduction (TPR) experiments were carried out with a Micromeritics Autochem 2910 catalyst characterization system, equipped with a TCD. We pretreated fresh, dried samples by passing high-purity (99.9%) argon (20 ml/min) at 773 K for 3 h. After cooling to ambient temperature, the argon flow was replaced by 5% H_2/Ar mixture. The catalyst samples were heated in this atmosphere to 1273 K at a heating rate of 5 K/min. The flow rate of the H_2/Ar mixture was kept at 40 ml/min throughout the experiment. The water produced during the reduction was condensed in a cold trap immersed in a slurry of isopropanol and liquid nitrogen. The amount of catalyst used in these experiments was adjusted so that samples contained equivalent amounts of V_2O_5 in all of the experiments.

Diffuse-reflectance UV–vis spectra were recorded in the range of 200–800 nm at 523 K with an Ocean Optics HR2000 CCD array spectrophotometer equipped with a R200-7 reflection/backscattering probe. The samples were pressed into 1-mm-thick pellets and placed on a heater for in situ heating. After allowing the sample to equilibrate at the required temperature (523 K), we made measurements by placing the probe at a right angle to the pellet with the help of an anodized aluminum holder. The reflectance spectra were converted into the Kubelka–Munk function, $F(R)$, which is proportional to the absorption coefficient for low values of $F(R)$.

X-ray photoelectron spectra were acquired on a VG Microtech Multilab ESCA 3000 spectrometer with the use of a nonmonochromatized Mg-K_α X-ray source ($h\nu = 1253.6$ eV) on in situ scraped fresh catalyst pellets at room temperature. Selected spectra were also recorded with Al-K_α X-ray ($h\nu = 1486.6$ eV) to eliminate the overlap between different Auger and core levels. Base pressure in the analysis chamber was maintained in the range of 6×10^{-10} Torr. The energy resolution of the spectrometer was determined from the full width at half-maximum of metallic gold, and the value obtained was better than 0.8 eV for Mg-K_α radiation and 1.1 eV for Al-K_α radiation, respectively, at a pass energy of 20 eV.

^{51}V MAS NMR experiments were performed at 131.54 MHz on a Bruker DRX-500 NMR spectrometer with a Bruker broad-band CP-MAS probe. The samples were spun at 8, 10, or 12 kHz with 4-mm-diameter zirconia rotors. A pulse length of 3 μs and a recycle delay of 500 ms were used for acquisition of the data.

Catalytic reactions were carried out in a fixed-bed, downflow glass reactor at atmospheric pressure. About 2 g of catalyst was placed at the center of the reactor with quartz wool plugs. Ethylbenzene was fed into the reactor with a high-pressure syringe pump (Isco; Model 500 D). N_2O was introduced into the reactor at desired flow rates with a mass flow controller (Hi-Tech; Bronkhorst).

Condensed reaction products (styrene, benzene, toluene, styrene oxide) were analyzed with a Hewlett-Packard 6890 plus gas chromatograph equipped with a flame ionization detector and a capillary column (BPX5, length 50 m, i.d. 0.32 mm). The gaseous products were analyzed online with a Chemito-1000 gas chromatograph equipped with TCD, with the use of a spherocarb column (mesh size 80/100, 8′, 1/8″

dia). Specific activities ($mol_{EB}\,h^{-1}\,m^{-2}$) and turnover rates $\{mol_{EB}\,mol_V^{-1}\,s^{-1}\}$ were calculated from conversion values of ethylbenzene (X_{EB}), with the use of specific surface areas and vanadium contents of the samples, respectively.

3. Results and discussion

3.1. Catalytic activity

Fig. 1 shows the yield of styrene and selectivities of other products observed at 623 K in nitrous oxide and nitrogen atmospheres for a $20VO_x/Al_2O_3$ sample. The reactions were performed under identical conditions, at an ethylbenzene space velocity of 1 h^{-1} and a N_2/N_2O space velocity of 1200 h^{-1}. It can be seen that the styrene yield in the presence of nitrous oxide is at least two times higher than that in nitrogen atmosphere at 623 K. The yield of styrene decreased with reaction time for both N_2O and N_2 atmospheres. However, the yield remained at a much higher level in N_2O throughout the period studied. The decrease in the yield of styrene could be attributed to two factors: an increase in the oxidation of styrene to styrene oxide and a rapid deactivation of the catalyst. A higher selectivity for styrene oxide was observed in the N_2O atmosphere, probably because of the availability of oxygen through the dissociation of N_2O. The selectivity for styrene oxide increased with time on stream, because of the increasing rate of styrene epoxidation in the presence of excess N_2O.

The selectivities for benzene and toluene, which are the dealkylation products of ethylbenzene, were lower in N_2O than in N_2. Although the dealkylation of EB in the presence of N_2O remained more or less at a constant level, it was higher and increased with time on stream in N_2. Fig. 2 compares styrene yields of the rest of the three catalysts, viz., 2, 5, and 10% vanadia-loaded catalysts, in the presence of N_2O and N_2. Styrene yield was the highest on $10VO_x/Al_2O_3$ catalyst, in the presence of N_2O, whereas on $2VO_x/Al_2O_3$, it was the lowest. Similar to the observation for $20VO_x/Al_2O_3$, initial deactivation was also observed for catalysts with other vanadia loadings. However, $10VO_x/Al_2O_3$ catalyst exhibits the highest styrene yield at any time on stream. Simultaneously, styrene oxide yield increased on all of the catalysts with time on stream (not reported in the figure), but it was found to be the highest on $2VO_x/Al_2O_3$ catalyst.

Fig. 3 presents the effect of variation of reaction temperature on the styrene yield in N_2O atmosphere at a time on stream of 2 h. The EB conversion and styrene yield increase monotonically with increasing temperature, for the time period they were studied. At 623 K, the conversion of ethylbenzene and the yield of styrene were low, at 15 and 13 mol%, respectively. However, when the temperature was increased to 673 K, their values were more than doubled. With increasing temperature, the selectivity for styrene oxide decreased, whereas that for the dealkylation products,

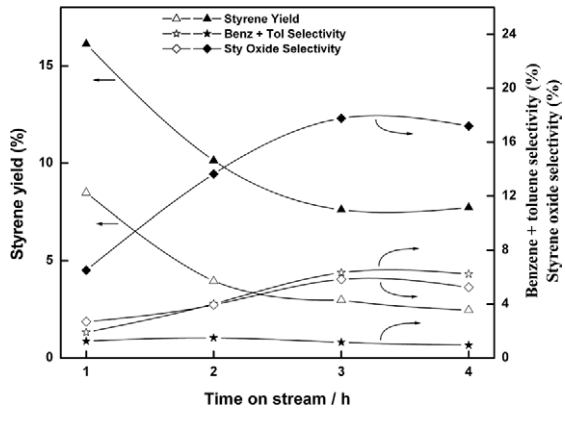

Fig. 1. The yield of styrene and selectivities of benzene, toluene, and styrene oxide in nitrogen and nitrous oxide atmospheres as a function of time on stream. Reaction temperature, 623 K; WHSV of EB, 1; N_2/N_2O flow rate, 1200 h^{-1}; 20 VO_x/Al_2O_3. Solid symbols, under N_2O flow; open symbols, under N_2 flow; (△,▲) styrene yield; (☆,★) sum of benzene and toluene selectivities; (◇,◆) styrene oxide selectivity.

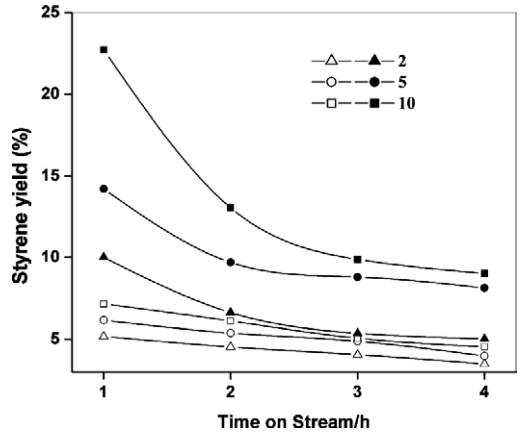

Fig. 2. Variation of styrene yield with time on stream on various VO_x/Al_2O_3 catalysts. Reaction temperature, 623 K; WHSV of EB, 1; N_2/N_2O flow rate, 1200 h^{-1}; Solid symbols, under N_2O flow; open symbols, under N_2 flow; (△,▲) $2VO_x/Al_2O_3$; (○,●) $5VO_x/Al_2O_3$; (□,■) $10VO_x/Al_2O_3$.

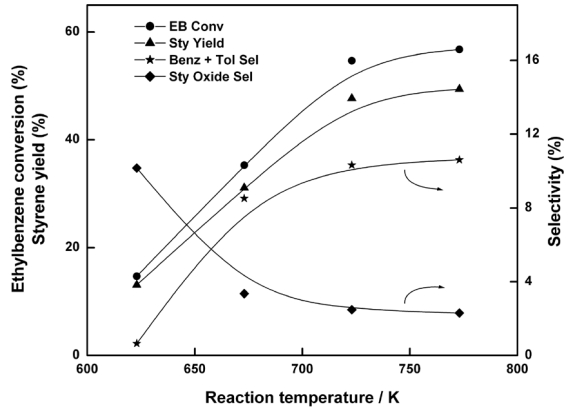

Fig. 3. Effect of temperature on product yields. $5VO_x/Al_2O_3$; reaction time, 2 h; N_2O flow rate, 1200 h^{-1}; WHSV of EB, 1; (●) ethylbenzene conversion; (▲) styrene yield; (★) sum of benzene and toluene selectivities; (◆) styrene oxide selectivity.

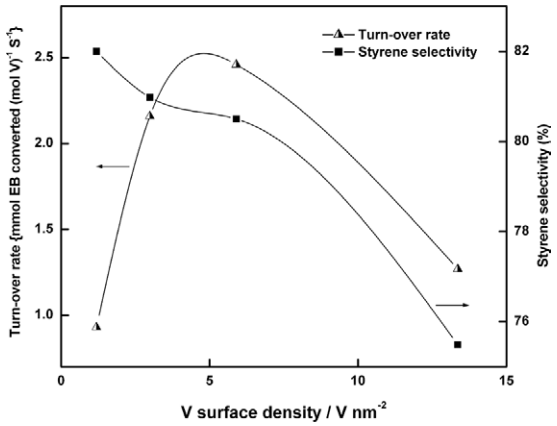

Fig. 4. Effect of VO_x surface density on the initial rate of ethylbenzene conversion at 673 K normalized per V atom (▲) and the selectivity of styrene extrapolated to zero conversion (■).

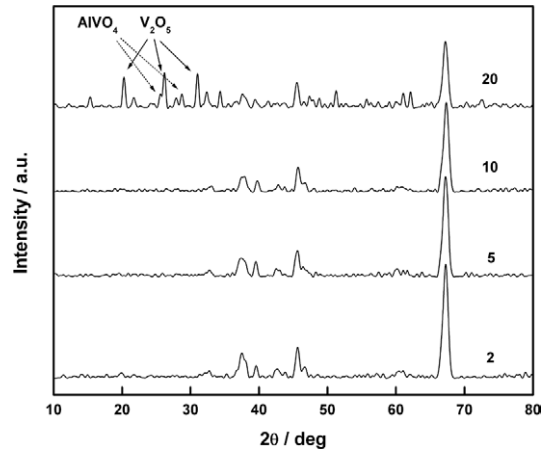

Fig. 5. Powder X-ray diffraction patterns of calcined VO_x/Al_2O_3 catalysts as a function of vanadia loading in wt%.

benzene and toluene, increased. Hence, higher temperatures cause higher dealkylation of ethylbenzene and lower yield of styrene oxide despite the presence of nitrous oxide. These trends in activity and selectivity were similar for catalysts with other vanadia loadings as well. The activity of bulk V_2O_5 catalysts was very low under these experimental conditions.

The effect of vanadium surface density on the initial rate of ethylbenzene conversion per vanadium atom (extrapolated to zero residence time) at 673 K is shown in Fig. 4. The apparent turnover rate increased as the surface density increased and reached a maximum at a vanadium surface density of 6 V nm^{-2}. The rate decreased thereafter when the surface density increased to 13.4 V nm^{-2}. The variation in styrene selectivity at zero conversion of ethylbenzene is also shown in Fig. 4 as a function of vanadium surface density. The selectivity for styrene decreased as the vanadium surface density increased. The selectivity for styrene oxide also decreased, whereas dealkylation products, benzene and toluene, increased with increasing surface density (not shown).

3.2. Catalyst characterization

Table 1 shows the vanadium content of calcined VO_x/Al_2O_3 catalysts determined from ICP-AES analysis, BET surface areas, and VO_x surface densities calculated with the use of these two parameters. The specific surface area decreased with increasing vanadium content. Fig. 5 shows the XRD patterns of VO_x/Al_2O_3 catalysts with different vanadia loadings. For vanadia loadings up to 10 wt%, only the peaks characteristic of γ-Al_2O_3 ($d = 1.4$, 2.0, and 2.4 Å, JCPDS 10-425) were observed. For the catalyst containing 20 wt% V_2O_5, well-defined peaks at $d = 4.4$, 3.4, and 2.9 Å corresponding to crystalline V_2O_5 (JCPDS 9-387) appeared in the XRD pattern. The $20VO_x/Al_2O_3$ sample also exhibits weak X-ray reflections at $d = 3.5$, 3.1, and 3.2 Å, corresponding to aluminum orthovanadate, $AlVO_4$ (JCPDS 39-276), which is the only stable compound in the binary Al_2O_3–V_2O_5 system. The absence of any vanadia or vanadate peaks for catalysts with 2–10 wt% vanadia loadings may be due to the high dispersion of vanadia on Al_2O_3 surface at these loadings with particle sizes lower than the detectable limit of XRD.

The volume-averaged particle size of the alumina support in the different catalysts was calculated with the Debye–Scherrer equation. The most intense peak of γ-Al_2O_3 ($d = 1.40$) was considered for this purpose. The particle sizes were found to be around 12 nm for VO_x/Al_2O_3 catalysts calcined at 823 K and did not vary significantly with vanadia loading (Table 1).

Table 1
Characteristics of alumina support and supported vanadia catalysts studied

Sample	V content (ICP, wt%)	Surface area ($m^2\,g^{-1}$)	VO_x surface density ($VO_x\,nm^{-2}$)	Particle size (nm)	UV–vis absorption edge energy (eV)	H_2 TPR			XPS	
						$T_{max\,1}$ (K)	$T_{max\,2}$ (K)	Total H_2 consumption ($\mu mol\,H_2\,g^{-1}$)	V $2p_{3/2}$ binding energy (eV)	(V/Al) surface
Al_2O_3	0	113	0	12.33	–	–	–	–	–	–
$2VO_x/Al_2O_3$	1.06	105	1.19	12.39	3.3	757	–	138	517.3	0.004
$5VO_x/Al_2O_3$	2.58	102	2.99	12.37	2.92	743	–	467	517.7	0.015
$10VO_x/Al_2O_3$	4.74	95	5.90	11.99	2.41	724	–	1494	517.5	0.063
$20VO_x/Al_2O_3$	9.16	81	13.36	12.64	2.26	733	854	2412	517.2	0.075

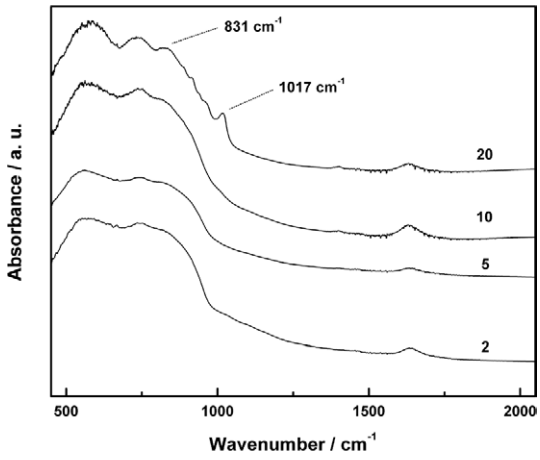

Fig. 6. FTIR spectra of calcined VO_x/Al_2O_3 catalysts as a function of vanadia loading in wt%.

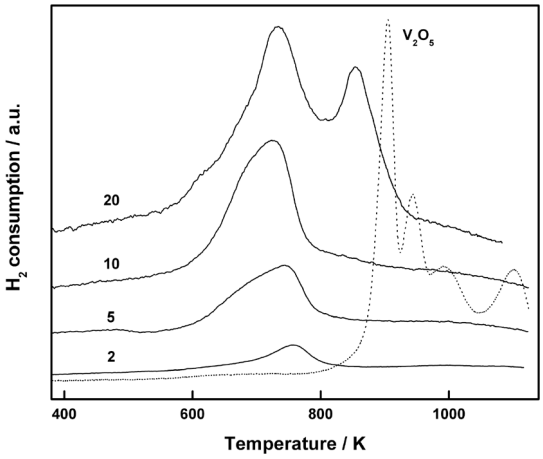

Fig. 7. TPR profiles of bulk V_2O_5 and calcined VO_x/Al_2O_3 catalysts. 5% H_2–Ar; heating rate, 5 K/min; flow rate, 40 ml/min.

FTIR spectra for calcined catalysts with different vanadia loadings are shown in Fig. 6. Although no characteristic peaks were observed for catalysts with vanadia loading up to 10 wt%, the spectrum of $20VO_x/Al_2O_3$ showed two bands centered at 1017 and 831 cm^{-1}. The first band corresponds to V=O stretching vibration, and the latter corresponds to V–O–V bending vibration [44]. The occurrence of these two bands, which are characteristic of V_2O_5 species, confirm the presence of well-defined vanadia crystallites on $20VO_x/Al_2O_3$, which is also observed by XRD.

The TPR profiles of bulk V_2O_5 and calcined VO_x/Al_2O_3 catalysts are presented in Fig. 7. The reduction profile for bulk V_2O_5 exhibited four major peaks at 905, 945, 998, and 1103 K. Bosch et al. [27] and Koranne et al. [29] have reported observing similar multiple major reduction peaks when bulk V_2O_5 was treated in 5% H_2 in argon up to 1273 K. The presence of multiple peaks is attributed to the reduction of V_2O_5 to V_2O_3 through intermediate formation of compounds with various oxidation states. A broad, minor reduction peak is also observed between 580 and 750 K. The reduction profiles for bulk vanadia reported in the literature vary widely, probably because of the differences in method of preparation, level of impurities, partial pressure of H_2 used, rate of heating, and reduction conditions [29].

The TPR profiles of catalysts with vanadia loadings of 2–10 wt% reveal a broad reduction peak, below 773 K (Fig. 7). The temperature peak maximum (T_{max}) was 757 K for $2VO_x/Al_2O_3$, and with an increase in vanadia content up to 10 wt%, the T_{max} values shifted to lower temperatures (Table 1). This shift actually results from the growth of the peak in the low-temperature side with increasing vanadium content. The peaks may be attributed to the reduction of monomeric, dimeric, or low oligomeric surface vanadia species [25,28,29]. The shift in T_{max} to lower temperatures (or, more correctly, the growth of a peak in the low-temperature side) with increasing vanadium content from 2 to 10 wt% may be ascribed to the progressive increase in polymeric vanadium species. These are more easily reducible than the monomeric species, probably as a result of weaker vanadium–oxygen bonds. Similar behavior has already been described by earlier workers [20,45]. The H_2 consumption (Table 1) increased with increasing vanadia loading from 2 to 10 wt%. However, this increase in H_2 consumption is not linear with vanadia loading. We attribute this to the ease of reduction of the vanadia species present at high vanadia loadings. This can be clearly seen from the shift in the T_{max} to lower temperatures. Better reducibility results in higher H_2 consumption per vanadium at higher loadings.

The catalyst $20VO_x/Al_2O_3$ displayed two major reduction peaks (Fig. 7). The T_{max} of the first peak (734 K) is in the range of values that are observed for lower vanadia loadings and can be attributed to the reduction of polymeric vanadia species. The T_{max} of the second peak corresponds to a higher reduction temperature (855 K). This peak can be assigned to the reduction of bulk-like V_2O_5 crystallites. This is in accordance with XRD and IR results, which show the presence of V_2O_5 crystallites with a size greater than 4 nm for the $20VO_x/Al_2O_3$ sample. The T_{max} of this peak is lower than the temperature of the lowest reduction peak observed for pure bulk V_2O_5, as bulk vanadia is more difficult to reduce because of increased diffusional limitations [29].

Fig. 8A shows the V $2p_{3/2}$ photoelectron spectra of calcined VO_x/Al_2O_3 catalysts as a function of vanadia loading. Secondary radiations of Mg/Al-K_α lead to a satellite peak of O 1*s* at lower binding energy that overlaps with the V 2*p* core level peaks in the 515–525-eV range. This satellite peak of O 1*s* is subtracted from the original spectra to obtain the V 2*p* contribution alone. The V $2p_{3/2}$ peaks appear around 517 eV, and the corresponding spin-orbit doublet, $2p_{1/2}$, appears at about 524.5 eV. The V $2p_{3/2}$ core level binding energy value of bulk V_2O_5 ($3d^0$) is reported to be around 517 eV [46], and this value decreases, as expected from the increase in the number of 3*d* electrons, for lower oxidation state vanadium compounds. The binding energy values of the present series of catalysts (Table 1) indicate that the vanadia surface species are fully oxidized (V^{5+}). Surface V/Al atomic ratios were calculated with the method

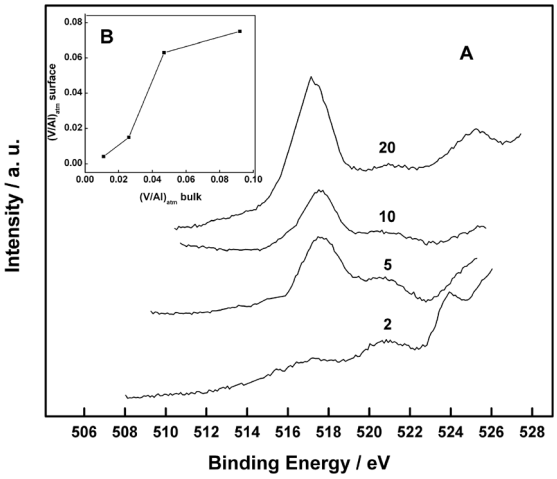

Fig. 8. (A) V $2p$ core-level spectra of calcined VO_x/Al_2O_3 catalysts, after satellite subtraction, as a function of vanadia loading. Integers in figure indicate vanadia loading in wt%. (B) Surface atomic ratio of V/Al obtained by XPS as a function of bulk atomic ratio. V $2p_{3/2}$ and Al $2p$ were used to determine surface atomic ratio by XPS.

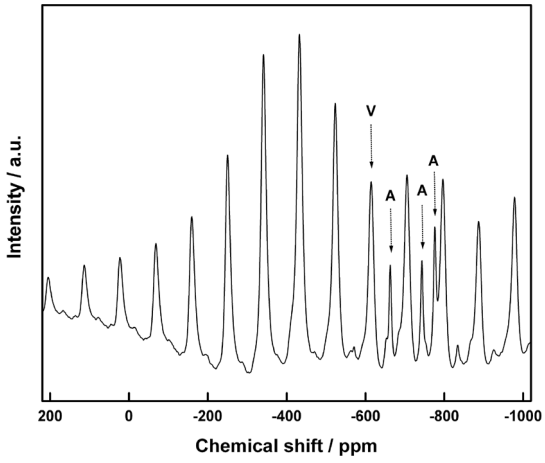

Fig. 9. ^{51}V MAS NMR spectrum of the calcined $20VO_x/Al_2O_3$. The alphabets 'A' and 'V' denote isotropic peaks of $AlVO_4$ and V_2O_5, respectively.

described by Gopinath and Raja [47], with the use of XPS peak intensities of V $2p_{3/2}$ and Al $2p$ and the corresponding photoionization cross-section values [48] for all vanadia loadings, and are included in Table 1.

Fig. 8B shows V/Al surface atomic ratios obtained by XPS plotted as a function of the total (bulk) V/Al atomic ratio of the catalysts determined by ICP-AES. The surface atomic ratio increases sharply up to a bulk atomic ratio of 0.05 (10 wt% vanadia loading) and thereafter increases only marginally. This indicates that multilayerd vanadia structures appear beyond a vanadia loading of 10 wt%.

The ^{51}V MAS NMR spectrum of $20VO_x/Al_2O_3$ confirms the presence of both $AlVO_4$ and bulk-like V_2O_5. The isotropic chemical shift values, which we determined by spinning the sample at different rates, are −614, −663, −744, and −774 ppm (Fig. 9). The isotropic peak observed at −614 ppm can be attributed to bulk-like V_2O_5, since

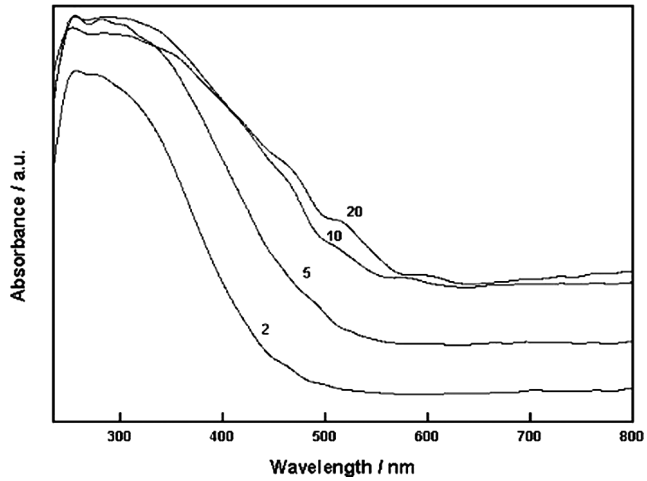

Fig. 10. UV–vis spectra of calcined and dehydrated VO_x/Al_2O_3 samples as a function of vanadia loading in wt%.

the position and side-band pattern of this peak are in good agreement with those reported for V_2O_5 in the literature. Eckert and Wachs [25] reported a δ_{iso} value of −609 ppm for V_2O_5. XRD studies have indicated that only one type of vanadium site and three different oxygen sites exist in crystalline V_2O_5 [49]. The isotropic peaks at −663, −744, and −774 ppm can be attributed to the presence of $AlVO_4$. The V species in $AlVO_4$ is in a tetrahedral $Q^{(0)}$ coordination, and the δ_{iso} values reported by Eckert and Wachs [25] are −661, −745, and −775 ppm. The values determined in our experiment are in good agreement with these values. The structure of $AlVO_4$, which was determined by a combination of simulated annealing and Rietveld refinement [50,51], contains three distinct VO_4^{3-} tetrahedra, two AlO_6 octahedra, and a pentacoordinated AlO_5 unit. The presence of three different vanadium (V) tetrahedra explains the origin of three isotropic peaks for vanadia species [50].

The low-energy charge-transfer (LCT) bands in the UV–vis spectrum, originating from charge transfer between vanadium and oxygen, are strongly influenced by coordination and/or the oxidation state of the vanadium ions and are usually observed in the 250–500-nm region for vanadium (V^{5+}) ions [13,45,52–56]. The d–d transition of V^{4+} (d^1) gives a broad band in the 550–850-nm region.

UV–vis spectra for calcined VO_x/Al_2O_3 catalysts, recorded at 523 K, are presented in Fig. 10. All of the catalysts exhibit broad band below ∼ 550 nm, characteristic of charge transfer transition from oxygen to vanadium (V), as described above. The spectrum of $2VO_x/Al_2O_3$ showed a wide band at about 255 nm. The spectrum observed for $5VO_x/Al_2O_3$ exhibited a shoulder around 350 nm. This shoulder is found to grow with increasing vanadium content. The observed red-shift and the relative increase in the band at 350 nm indicate an increase in the degree of vanadium condensation and hence an increase in the amount of oligomeric vanadia species with vanadia loading.

Absorption band edge energies can be used to quantify the electronic properties of solids and to correlate them with

catalytic activities. Edge energy values, which can be determined with the use of Tauc's law [57], have been used previously to characterize the domain sizes of VO_x, WO_x, and MoO_x in catalytic solids and to correlate catalytic activities [40,41,58–61]. The edge energies for the present series of catalysts were determined with Tauc's law from the intercept of a straight line fitted through the rise of the function $[F(R\alpha)h\nu]^2$ plotted versus $h\nu$ [59], where $F(R\alpha)$ is a Kubelka–Munk function [59] and $h\nu$ is the energy of the incident photon. The values obtained for the dehydrated catalysts are listed in Table 1. The edge energy is 3.3 eV for the $2VO_x/Al_2O_3$ sample, which decreases to 2.26 eV with increasing vanadia to 20 wt%. Higher edge energy values of about 3.3 eV are attributable to V^{5+} in monomeric tetrahedral coordination. Polymerization of VO_4 or VO_6 units tends to lower the edge energy values. The value of 2 eV is typical of bulk V_2O_5, which has V^{5+} in distorted tetragonal pyramidal coordination. The decrease in edge energy with increasing vanadia content indicates increased polymerization. The values for the present series of catalysts suggest that monomeric vanadium (V) species are the predominant species on the surface of $2VO_x/Al_2O_3$, and with increasing vanadium loading there is an increase in the degree of polymerization of vanadium (V) species. As is also obvious from the shift in the position of the bands toward higher wavelengths, the oligomerization ultimately leads to the appearance of octahedral polymeric species similar to that in bulk V_2O_5 for the $20VO_x/Al_2O_3$ catalyst.

Fig. 11 presents UV–vis spectra for the $20VO_x/Al_2O_3$ catalyst after reduction in H_2 and dehydrogenation reactions in the presence of N_2O and N_2. After reaction in a N_2 atmosphere at 673 K for 4 h, a weak, broad band between 500 and 800 nm (Fig. 11, spectrum b) is observed. This band can be assigned to forbidden d–d transitions of V^{4+} and/or V^{3+}, since it is clearly seen for $20VO_x/Al_2O_3$, after reduction in H_2 at 673 K for 4 h (Fig. 11, spectrum c). The band disappeared when the reduced sample was treated with N_2O at 673 K for 4 h, and the spectrum was similar to that of a fresh, calcined catalyst. The band is much more intense for the $20VO_x/Al_2O_3$ catalyst after dehydrogenation in a N_2 atmosphere, compared with that used in a N_2O atmosphere (Fig. 11, spectrum a); this shows the ability of N_2O to keep the active species at a higher oxidation state during the reaction.

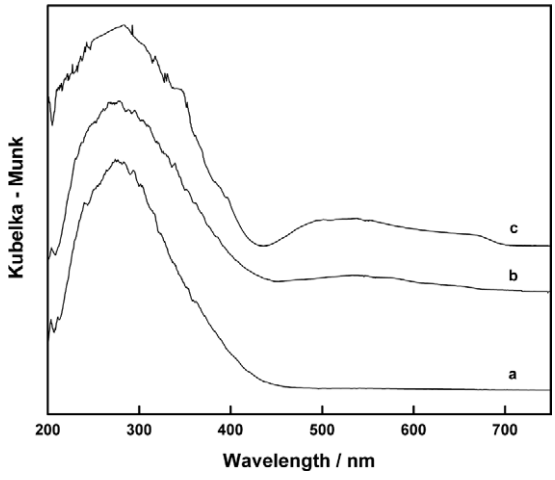

Fig. 11. UV–vis spectra of 20 VO_x/Al_2O_3 after (a) dehydrogenation reaction under N_2O flow at 673 K for 4 h (b) dehydrogenation reaction under N_2 flow at 673 K for 4 h (c) after reduction with H_2 at 673 K for 4 h.

4. Discussion

Various complementary characterization techniques show that the structure of dispersed VO_x species on an Al_2O_3 support depends on the VO_x surface density, as previously reported [25,39,40]. At low coverages (VO_x surface densities up to 6 V nm^{-2}), XRD does not detect any vanadium phase, whereas the catalyst with a surface density of 13.4 V nm^{-2} ($20VO_x/Al_2O^3$) shows peaks characteristic of bulk-like V_2O_5 and $AlVO_4$. UV–vis spectroscopy data suggest that vanadia exists as monomeric vanadium (V) species with tetrahedral coordination at a surface density of 1.2 V nm^{-2} ($2VO_x/Al_2O_3$). A decrease in absorption edge energy with increasing surface density indicates the progressive condensation of vanadia species, leading to polymeric V^{5+} species at higher loadings and finally to bulk-like vanadia crystallites at a surface density of 13.4 V nm^{-2}. TPR data show a shift in T_{max} to lower temperatures as the surface density increases from 1.2 to 6 V nm^{-2}, which may be attributed to the increased polymerization of vanadium species. These are more easily reducible than monomeric species. The additional peak observed at 855 K at a surface density of 13.4 V nm^{-2} can be ascribed to the reduction of bulk-like V_2O_5 crystallites. Consistent with this interpretation, a weak band at 1017 cm^{-1} characteristic of V=O stretching vibration is observed in the FTIR spectrum of the catalyst at a surface density of 13.4 V nm^{-2}. This band is not observed for catalysts with lower vanadia loadings. The values of surface atomic ratios obtained from XPS also indicate the formation of a multilayered vanadia phase only after 6 V nm^{-2}. Based on various characterization results, it can be concluded that monomeric tetrahedral V^{5+} species are predominant on the VO_x/Al_2O_3 catalyst at a surface density of 1.2 V nm^{-2}, polymerization of V^{5+} species increases as the surface density increases, and formation of bulk-like V_2O_5 crystallites takes place at a surface density of 13.4 V nm^{-2}.

The relationship observed between the turnover rate and vanadium surface density (Fig. 4) can be explained based on the degree of polymerization of vanadium species. The activity for the catalyst with a surface density of 1.2 V nm^{-2} is the lowest since the monomeric vanadia species, predominant on this catalyst, are less active than the polymeric V^{5+} species. In general, in oxidation reactions, the course of the reaction involves the oxidation–reduction cycles of V^{5+} species. The V–O–Al species appear to be more difficult to reduce than V–O–V or V=O sites in polymeric species. This

conclusion is also supported by the fact that the reducibility of the samples increases with an increase in vanadia loading from 2 to 10 wt%, as indicated by the shift in T_{max} to lower temperatures in TPR experiments (Fig. 7). The activity decreases again when a multilayer of polymerized V^{5+} species is formed on the surface, at higher surface densities (13.4 V nm^{-2}), which prevents the accessibility of the reactants to all of the vanadium ions. Hence, the maximum turnover rate is observed at intermediate surface densities corresponding to the formation of a vanadia monolayer on the surface of the support. The observation of a maximum in activity at an intermediate surface density was reported previously for the ODH of ethane and propane over vanadia catalysts supported on MgO [61–63], Al_2O_3, and ZrO_2 [40–42] and was attributed to the structure of the VO_x overlayer [41,42]. The observed dependence of the selectivities of the products on the surface density (Fig. 4) reveals that monomeric V^{5+} species are better suited for the dehydrogenation of ethylbenzene since the maximum selectivity for styrene is observed at the lowest surface density studied (1.2 V nm^{-2}). The bulk-like vanadia crystallites present at a surface density of 13.4 V nm^{-2} cause dealkylation of ethylbenzene, resulting in the increased formation of benzene and toluene.

The effect of N_2O in the dehydrogenation reaction is significant, as indicated by the higher styrene yield observed at 623 K compared with that in a N_2 atmosphere (Fig. 1). The vanadium species is continuously reduced during the reaction in N_2, whereas it is kept at a higher oxidation state when the reaction is carried out in a N_2O atmosphere, as seen from UV–vis spectral results (Fig. 11). The enhancement of the specific activity in the presence of N_2O is similar to the effect of CO_2 on the dehydrogenation reaction of ethylbenzene reported by Sakurai et al. [6]. This was termed the promoting effect of CO_2 by these authors and is ascribed to the ability of CO_2 to oxidize the reduced species during the reaction, which helps to keep it in a higher oxidation state. They observed an increase in styrene yield with an increase in the loading level of vanadium from 0 to 1.0 mmol/g of MgO, but a further increase in vanadium loading did not increase the styrene yield. According to Sakurai et al. [6], at low loadings, only isolated VO_4 species were dispersed over the MgO support, whereas at a loading of 3 mmol/g of MgO, polymeric V^{5+} species with bridging V–O–V oxide ions forming MgV_2O_6 and $Mg_2V_2O_7$ structures also coexist. To sum up, the degree of polymerization of vanadate species increases with loading level, leading to a concurrent increase in styrene yield.

The vanadium surface density required for a theoretical polyvanadate monolayer can be calculated as approximately 7 V nm^{-2} for the present system of catalysts. Below this surface density (vanadia loading 2–10 wt%), it is observed that turnover rates increase with increasing surface density (Fig. 4) and UV–vis absorption edge energies decrease (Table 1). Hence there is an inverse relationship between the turnover rates and the edge energies. This correlation, observed between the turnover rates and absorption edge energies, within monolayer coverage, is similar to that reported previously for small alkanes over two-dimensional transition metal oxides like VO_x, MoO_x, and WO_x dispersed over Al_2O_3, ZrO_2, and MgO [60]. For the ODH of propane, the turnover rates were found to increase in parallel with a decrease in the UV–vis absorption edge energies, and this was explained based on the activation energy for the dissociation of the first methylene C–H bond, which is the rate-determining step. The similarity in the relationship between turnover rate and absorption edge energy suggests that C–H bond dissociation of ethylbenzene proceeds via transition states requiring electron transfer from oxygen atoms to vanadium centers. The energy needed for this decides both the energy for C–H bond activation of ethylbenzene (which determines the turnover rate) and the energy at which absorption occurs in the UV–vis spectrum. The increase in the turnover rates with increasing surface density is accounted for by the fact that these electronic transitions require lower energies because of an increase in oxide domain size as the surface density increases. The accommodation of the transition state and the products in the rate-determining step requires two vanadium atoms bonded by a V–O–V bridge. This explains the lower turnover rates observed for catalysts that have low vanadia loadings, among which monomeric vanadium (V) is the predominant species (Fig. 4). Further work is in progress to investigate the applicability of these correlations to other supported oxide systems.

5. Conclusions

The catalytic properties of VO_x/Al_2O_3 catalysts with different vanadia loadings were evaluated in the oxidative dehydrogenation of EB in the presence of N_2O. Structural and surface characterization of these catalysts shows that the monomeric vanadium (V) species is predominant when vanadia loading is 2 wt%. With increasing vanadia loading, formation of polyvanadate species occurs, and at a vanadia loading of 20 wt%, V_2O_5 domains are observed along with $AlVO_4$ crystallites. The rate of ethylbenzene conversion per vanadium atom was found to increase with vanadia loading, reaching a maximum at 10 wt%, and decreases when the loading is increased further to 20 wt%. Structural and surface characterization data indicate that the most active form of the catalyst results when the surface of the support (Al_2O_3) is covered by two-dimensional polyvanadate species. The formation of bulk-like, vanadium-containing phases on the surface at higher loadings leads to a decrease in the activity as a result of the inaccessibility of a large fraction of vanadium atoms lying below the surface. The styrene yield was much higher in the presence of N_2O than that in a N_2 atmosphere, since the surface vanadium species are constantly kept at a higher oxidation state during the dehydrogenation with N_2O. Within the monolayer coverage of VO_x, the turnover rates for ethylbenzene increase in parallel with a decrease in the

UV–vis absorption edge energies. This suggests that the stability of the activated complex in the C–H bond dissociation step depends sensitively on the ability of the active oxide domains to transfer electrons from lattice oxygen to metal centers, as proposed in the case of ODH of propane.

Acknowledgments

NRS thanks CSIR, New Delhi, for a research fellowship. We thank Ms. Violet Samuel, Dr. Shubhangi Umbarkar, and Mr. S.C. Jha of the Catalysis Division, NCL, Pune, for various characterization studies. We also thank Dr. S. Sivasanker and Dr. A.V. Ramaswamy for helpful suggestions during the preparation of the manuscript.

References

[1] K.K. Kearby, in: P.H. Emmett (Ed.), Catalysis, vol. 3, Reinfold, New York, 1955, Chapter 10.
[2] E.H. Lee, Catal. Rev. 8 (1973) 285.
[3] C.R. Adams, T.J. Jennings, J. Catal. 17 (1970) 157.
[4] M. Sugino, H. Shimada, T. Turuda, H. Miura, N. Ikenaga, T. Suzuki, Appl. Catal. A 121 (1995) 125.
[5] T. Badstube, H. Papp, P. Kustrowski, R. Dziembaj, Catal. Lett. 55 (1998) 169.
[6] Y. Sakurai, T. Suzaki, K. Nakagawa, N. Ikenaga, H. Aota, T. Suzuki, J. Catal. 209 (2002) 16.
[7] Y. Sakurai, T. Suzaki, N. Ikenaga, T. Suzuki, Appl. Catal. A 192 (2000) 281.
[8] N. Ikenaga, T. Tsuruda, K. Senma, T. Yamaguchi, Y. Sakurai, T. Suzuki, Ind. Eng. Chem. Res. 39 (2000) 1228.
[9] S.E. Park, J.-S. Chang, V.P. Vislovskiy, M.S. Park, K.Y. Lee, J.S. Yoo, in: 6th International Conference on Carbon Dioxide Utilization, Breckenridge, USA, 2001, Preprinted Abstracts, p. 60.
[10] R. Dziembaj, P. Kustrowski, T. Badstube, H. Papp, Top. Catal. 11/12 (2000) 317.
[11] J.M. Lopez Nieto, A. Dejoz, M.I. Vazquez, W. O'Leary, J. Cunningham, Catal. Today 40 (1998) 215.
[12] P. Kustrowski, M. Zbroja, R. Dziembaj, H. Papp, Catal. Lett. 80 (2002) 1.
[13] E.V. Kondratenko, M. Baerns, Appl. Catal. A 222 (2001) 133.
[14] S. Kannan, Appl. Clays Sci. 13 (1998) 347.
[15] H.H. Kung, Adv. Catal. 40 (1994) 1.
[16] E.A. Mamedov, V. Corte's Corberan, Appl. Catal. A 127 (1994) 1.
[17] S. Albonetti, F. Cavani, F. Trifiro, Catal. Rev. Sci. Eng. 38 (1993) 43.
[18] T. Blasco, J.M. Lopez Nieto, Appl. Catal. A 157 (1997) 117.
[19] M.A. Banares, Catal. Today 51 (1999) 319.
[20] A.W. Stobbe-Kreemers, G.C. van Leerdam, J.-P. Jacobs, H.H. Brongersma, J.J.F. Scholten, J. Catal. 152 (1995) 130.
[21] K.V.R. Chary, G. Kishan, C. Praveen Kumar, G. Vidya Sagar, Appl. Catal. A 246 (2003) 335.
[22] C. Cristiani, P. Forzatti, G. Busca, J. Catal. 116 (1989) 586.
[23] G.T. Went, S.T. Oyama, A.T. Bell, J. Phys. Chem. 94 (1990) 4240.
[24] S.S. Chan, I.E. Wachs, L.L. Murrel, L. Wang, W. Keith Hall, J. Phys. Chem. 88 (1984) 5831.
[25] H. Eckert, I.E. Wachs, J. Phys. Chem. 93 (1989) 6796.
[26] T. Tanaka, H. Yamashita, R. Tsuchitani, T. Funabiki, S. Yoshida, J. Chem. Soc. Faraday Trans. 1 (1988) 84, 2987.
[27] H. Bosch, B.J. Kip, J.G. Van Ommen, P.J. Gellings, J. Chem. Soc. Faraday Trans. 80 (1984) 2479.
[28] Z. Sobalik, O.B. Lapina, O.N. Novgorodova, V.M. Mastikin, Appl. Catal. 63 (1990) 191.
[29] M.M. Koranne, J.G. Goodwin Jr, G. Marcelin, J. Catal. 148 (1994) 369.
[30] F. Roozeboom, M.C. Mittelmeijer-Hazeleger, J.A. Moulijn, J. Medema, V.H.J. De Beer, P.J. Gellings, J. Phys. Chem. 84 (1980) 2783.
[31] A. Haber, A. Kozlowska, R. Kozlowski, J. Catal. 102 (1986) 52.
[32] N.K. Nag, F.E. Massoth, J. Catal. 124 (1990) 127.
[33] M.A. Vuurman, I.E. Wachs, J. Phys. Chem. 96 (1992) 5008.
[34] I.E. Wachs, J. Catal. 129 (1991) 307.
[35] L.R. Le Coustumer, B. Taouk, M. Le Meur, E. Payen, M. Guelton, J. Grimblot, J. Phys. Chem. 92 (1988) 1230.
[36] I.E. Wachs, Chem. Eng. Sci. 45 (1990) 2561.
[37] I.E. Wachs, Catal. Today 27 (1996) 437.
[38] T. Blasco, A. Galli, J.M. Lopez Nieto, F. Trifiro, J. Catal. 169 (1997) 203.
[39] J.G. Eon, R. Olier, J.C. Volta, J. Catal. 145 (1994) 318.
[40] M.D. Argyle, K. Chen, A.T. Bell, E. Iglesia, J. Catal. 208 (2002) 139.
[41] A. Khodakov, J. Yang, S. Su, E. Iglesia, A.T. Bell, J. Catal. 177 (1998) 343.
[42] A. Khodakov, B. Olthof, A.T. Bell, E. Iglesia, J. Catal. 181 (1999) 205.
[43] B. Olthof, A. Khodakov, A.T. Bell, E. Iglesia, J. Phys. Chem. B 104 (2000) 1516.
[44] V. Dimitrov, Y. Dimitriev, A. Montenero, J. Non-Crystall. Sol. 180 (1994) 51.
[45] M.A. Centeno, P. Malet, I. Carrizosa, J.A. Odriozola, J. Phys. Chem. B 104 (2000) 3310.
[46] J.F. Moulder, W.F. Stickle, P.E. Sobol, K.D. Bomben, in: J. Chastain, R.C. King Jr. (Eds.), Handbook of X-ray Photoelectron Spectroscopy, Physical Electronics, Eden Prairie, 1995, p. 241.
[47] C.S. Gopinath, T. Raja, J. Phys. Chem. B 105 (2001) 12427.
[48] J.J. Yeh, I. Lindau, At. Data Nucl. Data Tables 32 (1985) 1.
[49] C.J. Fontenot, J.W. Wiench, G.L. Schrader, M. Pruski, J. Am. Chem. Soc. 124 (2002) 8435.
[50] U.G. Nielsen, A. Boisen, M. Brorson, C.J.H. Jacobsen, H.J. Jakobsen, J. Skibsted, Inorg. Chem. 41 (2002) 6432.
[51] A.A. Coelho, J. Appl. Crystallogr. 33 (2000) 899.
[52] G. Lischke, W. Hanke, H.-G. Jerchkewitz, G. Olmann, J. Catal. 91 (1985) 54.
[53] A. Corma, J.M. Lopez Nieto, N. Paredes, Appl. Catal. A 104 (1993) 161.
[54] M. Schraml-Marth, A. Wokaun, M. Pohl, H.L. Krauss, J. Chem. Soc. Faraday Trans. 1 (1991) 87, 2635.
[55] G. Centi, S. Perathoner, F. Trifiro, A. Aboukais, C.F. Aissi, M. Guelton, J. Phys. Chem. 96 (1992) 2617.
[56] A. Pantazidis, A. Burrows, C.J. Kiely, C. Mirodatos, J. Catal. 177 (1998) 325.
[57] J. Tauc (Ed.), Amorphous and Liquid Semiconductors, Plenum, London, 1974.
[58] D. Wei, G.L. Haller, in: Proceedings of 2nd Memorial G.K. Boreskov International Conference, Novosibirsk, 1997, p. 110.
[59] R.S. Weber, J. Catal. 151 (1995) 470.
[60] K. Chen, A.T. Bell, E. Iglesia, J. Catal. 209 (2002) 35.
[61] C. Pak, A.T. Bell, T. Don Tilley, J. Catal. 206 (2002) 49.
[62] D. Siew Hew Sam, V. Soenen, J.C. Volta, J. Catal. 123 (1990) 417.
[63] P.M. Michalakos, M.C. Kung, H.H. Kung, J. Catal. 140 (1993) 226.